EEG biomarkers of reduced inhibition in human cortical microcircuits in depression

Frank Mazza[1,2], Taufik A. Valiante[3,4,5,6,7,8,9], John D. Griffiths[1,9,10], Etay Hay[1,2,10]

[1]Krembil Centre for Neuroinformatics, Centre for Addiction and Mental Health, [2]Department of Physiology, University of Toronto, [3]Krembil Brain Institute, University Healthy Network, [4]Department of Electrical and Computer Engineering, University of Toronto, [5]Institute of Biomaterials and Biomedical Engineering, University of Toronto, [6]Department of Surgery, University of Toronto, [7]Center for Advancing Neurotechnological Innovation to Application, [8]Max Planck-University of Toronto Center for Neural Science and Technology, [9]Institute of Medical Sciences, University of Toronto, [10]Department of Psychiatry, University of Toronto

Abstract

Reduced cortical inhibition by somatostatin-expressing (SST) interneurons has been strongly associated with treatment-resistant depression. However, whether the effects of reduced SST interneuron inhibition on microcircuit activity have signatures detectible in electroencephalography (EEG) signals remains unknown. We simulated resting-state activity and EEG using detailed models of human cortical microcircuits with normal (healthy) or reduced SST interneuron inhibition (depression). Healthy microcircuit models showed emergent key features of resting-state EEG, and depression microcircuits exhibited increased theta, alpha and low beta power (4 – 15 Hz). The changes in depression involved a combination of an aperiodic broadband, and periodic theta and low beta components. We then demonstrated the specificity of the EEG signatures of reduced SST interneuron inhibition by showing they were distinct from those corresponding to reduced parvalbumin-expressing (PV) interneuron inhibition. Our study thus links SST interneuron inhibition level to distinct features in EEG simulated from detailed human microcircuits, which can serve to better identify mechanistic subtypes of depression using EEG, and non-invasively monitor modulation of cortical inhibition.

Corresponding author: Dr. Etay Hay
Krembil Centre for Neuroinformatics, Centre for Addiction and Mental Health
250 College St, Toronto, Ontario, M5T 1R8
Email: etay.hay@camh.ca

Introduction

Major depressive disorder (depression) is a leading cause of disability worldwide[1] and involves varying mechanisms and symptoms[2,3]. Consequently, a significant proportion of patients remain resistant to antidepressants[4] and second-line treatments[5]. Electro-encephalography (EEG) offers a non-invasive and cost-effective method for brain signal-based biomarkers to improve diagnosis, monitoring and treatment of depression subtypes[6,7]. However, the multi-scale mechanisms of depression and their link to clinically-relevant brain signals remain poorly understood.

There is growing evidence that reduced cortical inhibition plays a mechanistic role in treatment-resistant depression, especially inhibition mediated by somatostatin-expressing (SST) interneurons[8–13]. Recent studies showed a marked reduction in SST expression by SST interneurons in post-mortem tissue of depression patients, across all layers of the prefrontal cortex (PFC), indicating a decrease in SST interneuron inhibition[13–16]. In rodent models, silencing SST interneuron inhibition led to depression symptoms[12], and novel therapeutic compounds acting via positive allosteric modulation of alpha-5-gamma-aminobutyric-acid-A (α5-GABA$_A$) receptors targeted by SST interneurons resulted in pro-cognitive and anxiolytic effects[12,17]. In contrast, indications of changes in parvalbumin-expressing (PV) interneuron inhibition were inconsistent and less pronounced, signifying a more selective vulnerability for SST interneurons in depression[16,18]. Furthermore, other disorders such as Alzheimer's and aging that show changes in SST interneuron inhibition involve other key changes such as cell and synapse loss, therefore the altered inhibition may play a less central role in these conditions than in depression[19,20]. Changes in SST interneuron inhibition on circuit activity could have signatures detectible in EEG, due to this cell type's principal role in modulating input to pyramidal (Pyr) neurons, which are major contributors to EEG signals[8,21]. SST interneurons provide synaptic and tonic inhibition onto the apical dendrites of Pyr neurons[22,23], and mediate lateral inhibition in the cortex[8,24,25], particularly during periods of quiet, resting wakefulness (resting state)[26]. Accordingly, previous studies indicate that reduced SST interneuron inhibition in depression increases baseline activity of Pyr neurons[9,27].

While the contribution of SST interneurons to resting-state cortical oscillations remains largely unknown, studies show a role for this cell type in modulating low-frequency oscillations. SST stimulation entrains network activity in the 5 - 30 Hz range, and SST suppression modulates theta band (4 – 8 Hz) power[28,29]. SST interneurons have also been suggested to govern network synchrony in slow-wave sleep, which is marked by slow oscillations[30]. Thus, reduced SST interneuron inhibition in depression may affect EEG low-frequency power[31]. Conversely, PV interneurons have been shown to modulate high beta (20 – 30 Hz) and gamma (30 – 50 Hz) frequencies in human hippocampal LFP recordings, indicating that these two interneuron types likely modulate distinct frequency domains in recorded EEG[32,33]. We recently showed that a 40% reduction in SST interneuron inhibition, estimated from post-mortem tissue studies of depression patients[13], significantly increased baseline Pyr spike rate in simulated human microcircuits[27]. However, it is still unknown if this level of reduction in SST interneuron inhibition would significantly alter baseline oscillatory dynamics detectable in EEG.

Previous studies have linked neuronal spiking to extracellular signals, although mostly using animal models and local field potential (LFP)[34–37]. Human studies have characterized LFP oscillations in cortical slices and showed phase-amplitude coupling between deep and superficial layers[38]. Others have studied the phase preference of Pyr neuron spikes relative to spindle events in intracranial EEG oscillations[39,40]. However, experimental methods are limited in their ability to characterize the effects of the cellular changes in depression on human brain signals *in vivo*, thus meriting the use of computational models. Previous computational studies have identified inter-laminar mechanisms underlying evoked related potentials during stimulus response using simplified neuron morphologies and connectivity[41–43]. The increased availability of human data of the electrical properties of different neuron types and their synaptic connectivity[25,44,45] provides important constraints for detailed models of human cortical microcircuits[27], which can be used to link mechanisms of microcircuit activity in human health and disease to signatures in local circuit-generated EEG signals[42,46,47].

In this study, we identified EEG biomarkers of microcircuit effects due to reduced SST interneuron inhibition, as estimated from gene expression changes in depression. Using biophysically detailed models of human cortical microcircuits, we simulated resting-state activity in health and depression together with local EEG signals. We characterized changes in resting-

state EEG spectral power, and in relation to spiking activity in different neuron types, to identify biomarkers of reduced SST interneuron inhibition in depression.

Results

Human cortical microcircuit models reproduce resting-state EEG features

We used our previous detailed models of human cortical L2/3 microcircuits[27] (Fig 1a) as canonical cortical microcircuit models for simulating resting state spiking and EEG signals. The model microcircuits included the four key neuron types: Pyr neurons, SST interneurons, Parvalbumin-expressing interneurons (PV), and Vasoactive intestinal polypeptide-expressing interneurons (VIP). To simulate intrinsic healthy resting-state spiking activity, all neurons received random background excitatory input corresponding to baseline cortical and thalamic drive. The model microcircuits were implemented in a physical volume, enabling simulation of LFP and EEG together with microcircuit spiking (Fig 1a-d).

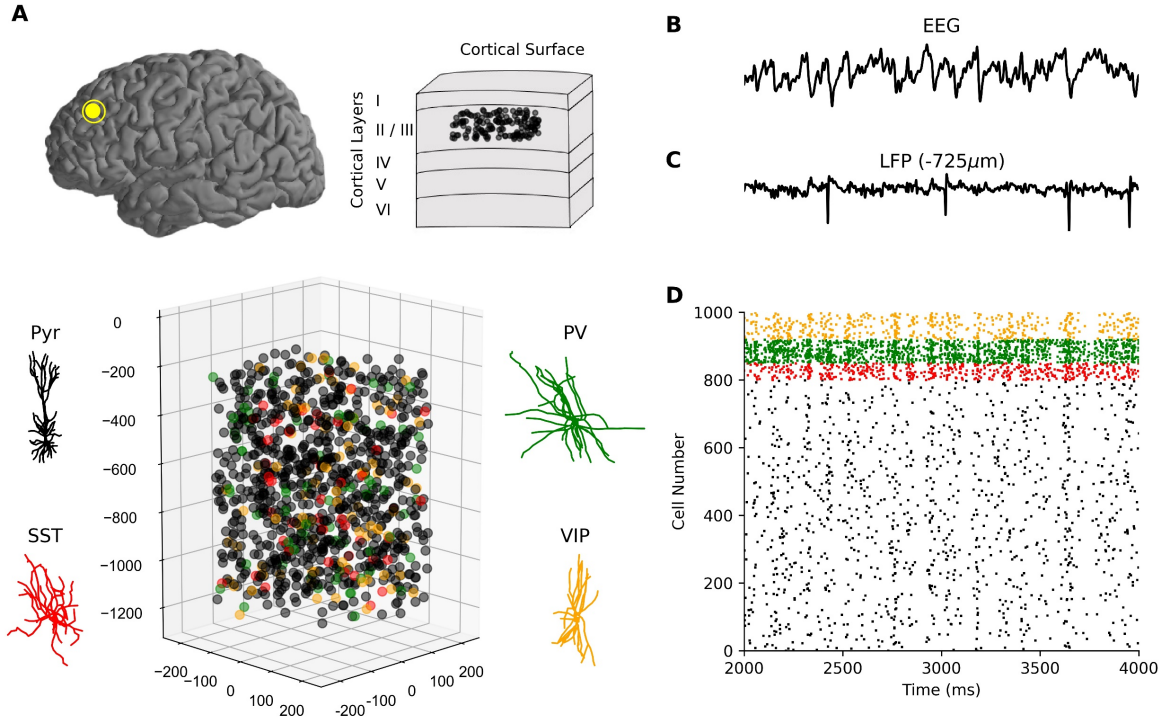

Figure 1. Simulating neuronal spiking and EEG signals from human cortical microcircuits. (a) Detailed models of human cortical microcircuits, showing somatic placement of 1000 neurons in a 500x500x950 μm^3 volume along layer 2/3 (250 - 1200 µm below pia) and reconstructed morphologies used in the neuron models. **(b – d)** Temporally aligned multi-scale simulated signals: EEG (b) from scalp electrode directly above the microcircuit; LFP signal (c) recorded at the middle of L2/3 (depth of -725 µm);

Raster plot of spiking in different neurons in the microcircuit (d), color-coded according to neuron type. Neurons received background excitatory inputs to generate intrinsic circuit activity.

Baseline microcircuit activity was oscillatory, marked by synchronous spiking events (Fig 1d) and corresponding fluctuations in LFP and EEG signals (Fig 1b, c). We quantified oscillatory activity in the healthy microcircuits by calculating EEG power spectral density (PSD). The microcircuits EEG exhibited a peak in theta (4 – 8 Hz) and alpha (8 – 12 Hz) bands (n = 60 randomized microcircuits, Fig 2a) and a 1/f background trend (Fig 2a, inset).. We then calculated spectrograms of circuit activity to analyze the evolution of signal strength in the time-frequency domain. The spectrograms showed 41 ± 3 transient theta-alpha events per 28 s simulation, with average duration of 181 ± 12 ms (Fig 2b). The circuit simulations thus reproduced several key temporal and spectral features of resting-state human EEG, such as an oscillatory peak power in theta and alpha bands and a background 1/f trend[48,49]. Critically, these oscillatory properties were emergent, and were not explicitly optimized for, which therefore constitutes an important validation of the model and demonstration of its ability to capture key properties of human cortical microcircuit dynamics.

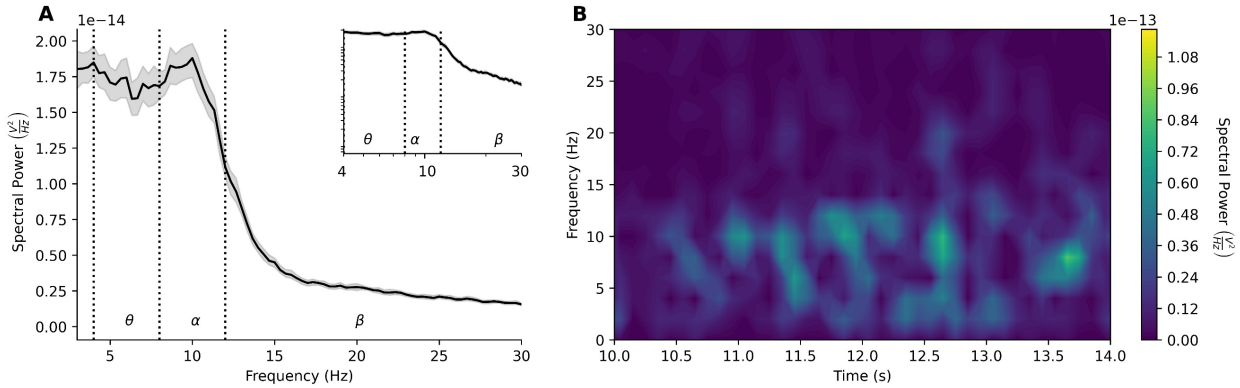

Figure 2. Models of human cortical microcircuits reproduce key features of resting-state EEG. (a) Power spectral density plot of circuit simulations (n = 60 randomized microcircuits, bootstrapped mean and 95% confidence intervals), exhibiting peak power in theta and alpha frequency bands. Inset – same power spectral density plot shown on log-log scale, illustrating the 1/f relationship between power and log frequency, inversely linear between 2-30 Hz with slope -0.99 ± 0.07. Frequency bands are delimited by dotted lines. **(b)** Example spectrogram of simulated microcircuit EEG, exhibiting theta and alpha events.

EEG biomarkers of reduced SST in depression microcircuits

We compared simulated EEG in healthy versus depression microcircuits using our previous depression models, in which SST synaptic and tonic inhibition were reduced (*n* = 60 randomized

microcircuits, Fig 3a). The simulated EEG from depression microcircuits exhibited a prominent peak in theta and alpha bands (4 – 12 Hz) similarly to the healthy microcircuits, but there was a significantly increased power in these bands and in low-beta frequencies (5 – 15 Hz, 56% increase on average, $p < 0.05$, Cohen's $d = 1.67$, Fig 3b). We decomposed EEG PSDs into aperiodic (Fig 3c) and periodic (Fig 3d) components, to compare the distinct functional components of the absolute PSDs. There was a 44% increase in aperiodic broadband power in depression compared to healthy microcircuits (5 – 30 Hz, $p < 0.05$, Cohen's $d = 4.9$), and a 30% reduction in aperiodic exponent (healthy = 0.99 ± 0.07, depression = 0.69 ± 0.07, $p < 0.05$, Cohen's $d = 2.6$). The periodic component of the PSDs from depression microcircuits showed a 35% increase in theta power (4 – 8 Hz, $p < 0.05$, Cohen's $d = 1.0$), and 62% increase in low-beta power (12 – 15 Hz, $p < 0.05$, Cohen's $d = 1.9$), but no significant change in alpha power compared to healthy microcircuits. Thus, the absolute power increase involved a combination of an aperiodic broadband component, and a periodic theta and low beta component.

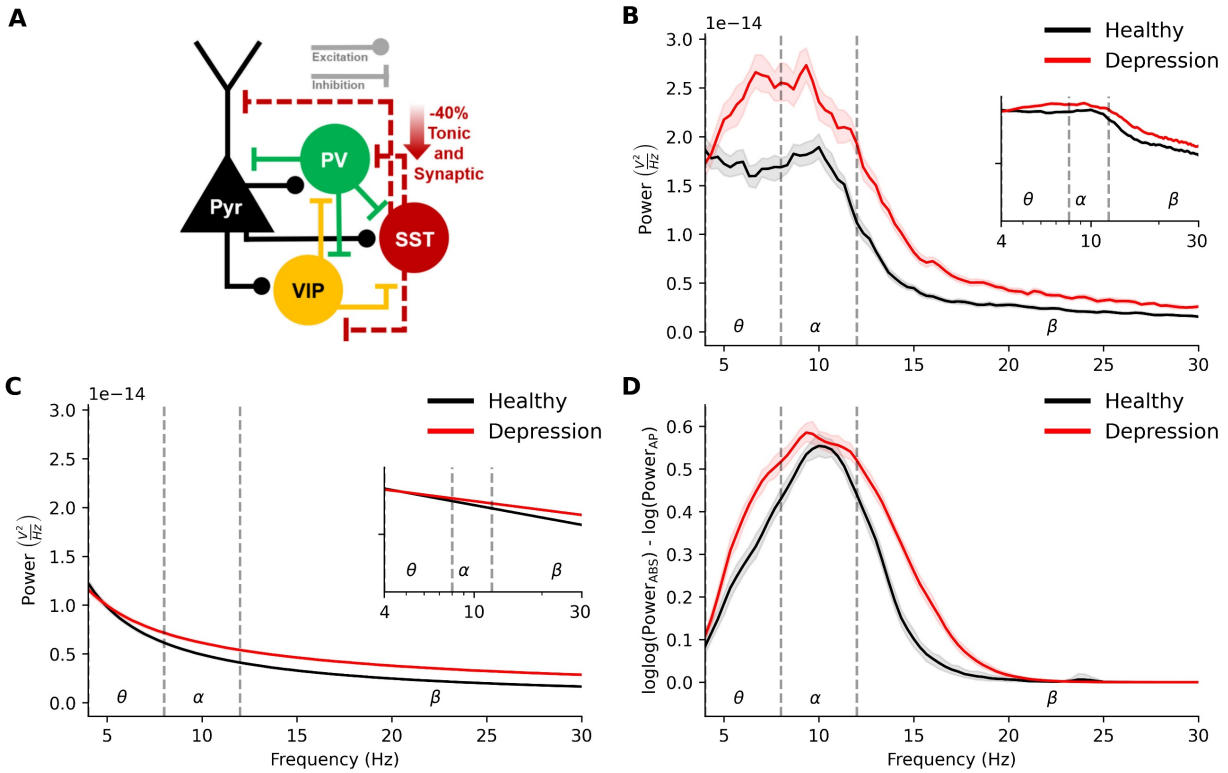

Figure 3. EEG signatures of reduced SST interneuron inhibition in depression microcircuit models. (a) Schematic connectivity diagram highlighting the key connections between different neuron types in the microcircuit. In the depression condition, dotted lines from the SST interneurons illustrate reduced synaptic and tonic inhibition onto different neuron types. **(b)** Power spectral density plot of simulated EEG from the healthy (black) and depression (red) microcircuit models (n = 60 randomized microcircuits per condition,

bootstrapped mean and 95% confidence interval). (**c**) Fitted aperiodic component of the PSD. **(d)** Fitted periodic component of the PSD.

To better establish the specificity of EEG biomarkers due to reduced SST interneuron inhibition, we simulated different levels of SST and PV interneuron inhibition reduction (20-60%) and compared their effects. For most levels of reduction (20 – 50%), spectral profiles of reduced SST interneuron inhibition were distinct from reduced PV interneuron inhibition (Fig 4a). PSDs from microcircuits with reduced PV interneuron inhibition were not significantly different from the healthy microcircuit PSD (20 - 50% reduction, 5 – 15 Hz, 1% change, $p = 0.48$), whereas PSDs from microcircuits with 20 – 50% reduced SST interneuron inhibition had significantly increased power (20% reduction, 5 – 15 Hz, 24 % increase, $p < 0.05$, $d = 0.89$: 50% reduction, 72% increase, $p < 0.05$, $d = 2.11$). Only in conditions of extreme inhibition reduction (60%), both SST and PV interneuron inhibition reduction showed a similarly extreme increase in 5-10 Hz power (SST: 70% increase, PV: 60% increase). Following spectral decomposition, we found that the aperiodic component also largely separated the two conditions (Fig 4b). Reduced PV interneuron inhibition microcircuits showed a decrease in broadband power (20% reduction: 9% decrease, $p < 0.05$, $d = 1.52$, 50% reduction: 28% decrease, $p < 0.05$, $d = 4.9$). and no change in aperiodic exponent, whereas reduced SST interneuron inhibition microcircuits showed an increase in broadband power (20% reduction: 23% increase, $p < 0.05$, $d = 2.7$, 50% reduction: 61% increase, $p < 0.05$, $d = 7.2$). In contrast, the periodic increases in power were largely similar between reduced PV and reduced SST interneuron inhibition conditions (Fig 4c, $p > 0.05$ for all reductions below 50%).

In terms of firing rate, microcircuits with reduced PV interneuron inhibition significantly increased baseline Pyr firing rate (healthy = 0.82 ± 0.03 Hz, 20% reduction: 0.91 ± 0.03 Hz, $p < 0.05$, $d = 2.05$, 40% reduction: 1.03 ± 0.04 Hz, $p < 0.05$, $d = 3.13$, 60% reduction: 1.34 ± 0.07 Hz, $p < 0.05$, $d = 5.03$), but to a lesser extent than reduced SST interneuron inhibition (20% SST = 1.03 ± 0.04 Hz, 40% SST = 1.28 ± 0.05 Hz, 40% PV = 1.03 ± 0.04 Hz, $p < 0.05$, $d = 11.8$). Thus, reduced SST interneuron inhibition affected baseline microcircuit activity to a greater extent than reduced PV interneuron inhibition.

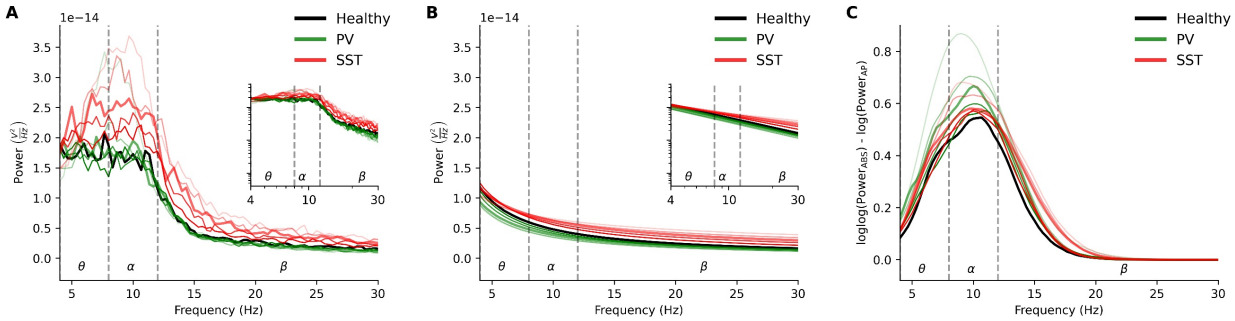

Figure 4. Reduced SST interneuron inhibition leads to distinct EEG signatures compared to reduced PV interneuron inhibition. (a) Power spectral density plot of simulated EEG from healthy (black), reduced SST (depression, red), and reduced PV (green) interneuron inhibition microcircuits, with decreasing opacity showing decreased inhibition for 20, 30, 40, 50, and 60% reduced inhibition models (n = 30 randomized microcircuits per condition, bootstrapped mean). (**b**) Fitted aperiodic component of the PSDs shown in a. **(c)** Fitted periodic component of the PSD shown in a.

We identified relationships between neuronal spiking and EEG spectral changes in depression microcircuit models by determining the EEG phase preference of the neuronal populations. The EEG time series were bandpass filtered from 4 – 12 Hz since the periodic component of the PSDs showed equally prominent theta and alpha components (Fig 5d). Spike time was then converted to phase of EEG signal by temporally aligning the bandpass-filtered signal to the angle of its Hilbert transform (Fig 5a-c). In healthy microcircuits, spiking in all neuronal types exhibited preference to the phase preceding the trough of the EEG waveform (Rayleigh's $p < 0.05$; Pyr = 269 ± 3°, SST = 267 ± 5°, PV = 283 ± 3°, VIP = 290 ± 2°). Depression microcircuits followed a similar phase preference (Rayleigh's $p < 0.05$; Pyr = 281 ± 2°, SST = 278 ± 5°, PV = 294 ± 3°, VIP = 296 ± 3°), but there was a decrease in preference selectivity, as quantified by population spike concentrations about the preferred phase (kurtosis, $p < 0.05$ for all; % decrease: Pyr = 10%, $d = 1.9$; SST = 17%, $d = 1.7$; PV = 19%, $d = 3.2$, VIP = 24%, $d = 4.8$).

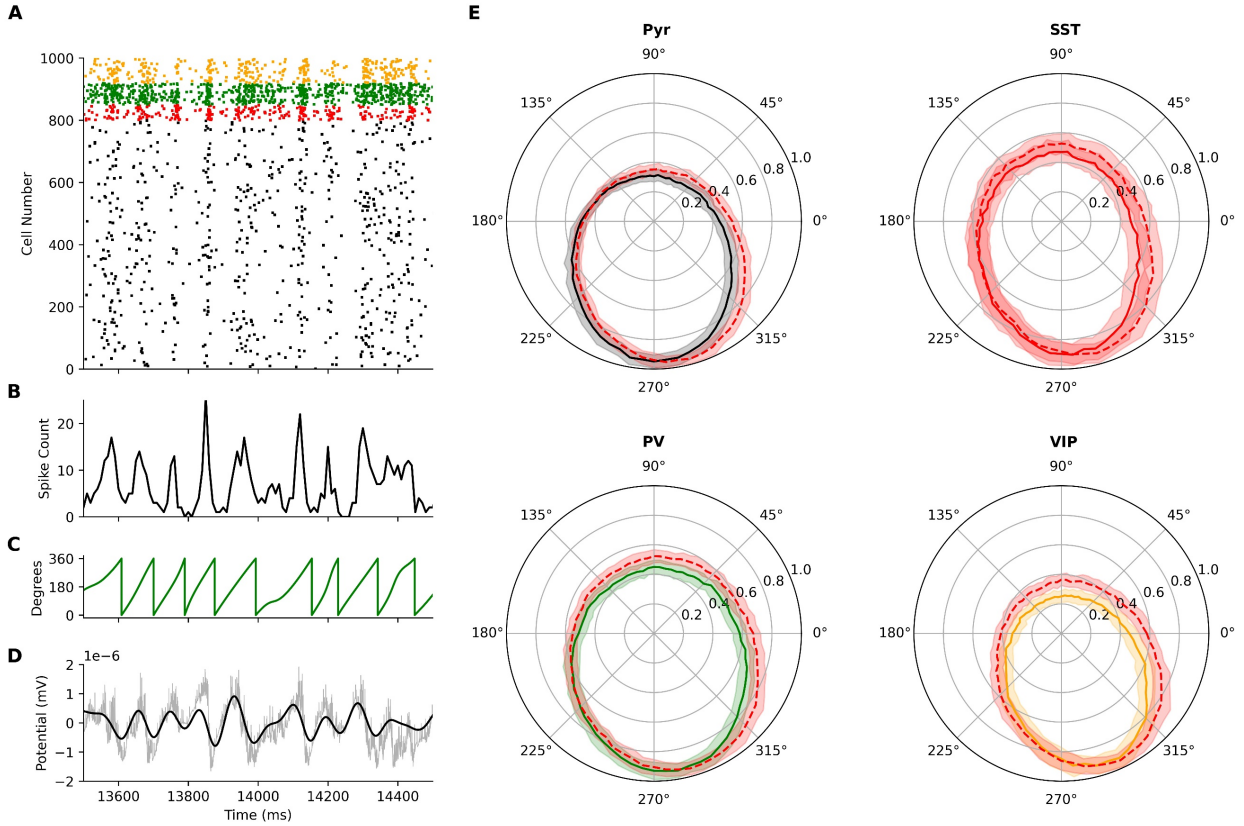

Figure 5. EEG phase preference of neuronal spiking in health and depression microcircuit models. **(a-d)** Temporally aligned simulated microcircuit signals used in calculating population phase-preference. **(a)** Raster plot of spiking in an example healthy microcircuit model. **(b)** Pyr population spike counts, in 10 ms bins. **(c)** Instantaneous phase of the theta-alpha bandpass filtered EEG signal, with trough corresponding to 0˚. **(d)** Theta-alpha bandpass filtered EEG signal (black) and unfiltered EEG signal (gray). **(e)** Population spike counts relative to theta-alpha (4 – 12 Hz) bandpass filtered EEG from healthy (non-magenta) and depression microcircuits (magenta). Plots show bootstrapped mean and standard deviation normalized by peak spike count. Neuron type colors for the healthy microcircuits are as in Fig 1.

Lastly, we examined the spatial distribution of scalp-measured EEG signals generated by the microcircuit simulations using a realistic head model, and determined the distance at which it was indistinguishable from noise. Picking an example region that is also relevant to depression, we placed the simulated microcircuit dipoles into L2/3 of the dorsolateral PFC, at a location directly underneath 10-20 system electrode AF3 (6ig 5a), and used a forward solution based on a boundary-element model with realistic head geometry and conductivity to compute simulated EEG signals. The resulting time series were obtained at different electrode locations on the scalp (Fig 6b). Difference in theta-alpha power in depression versus healthy microcircuits showed a nonuniform decay over the scalp, which was steeper laterally compared to medially (c.f. contour lines in Fig 6c). A significant difference in power was only seen in electrodes corresponding to the

ventral portion of the left dlPFC (AF3, the electrode above source) and the left orbitofrontal cortex (FP1 and FPz - 29mm and 46mm from source, respectively). The EEG biomarkers corresponding to microcircuit changes in depression were therefore mostly localized spatially.

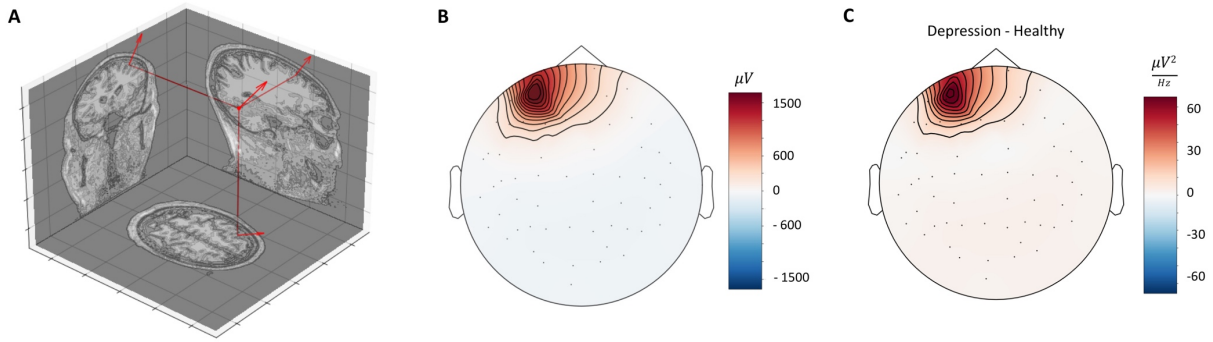

Figure 6: Topographic distribution of microcircuit EEG signal in a realistic head model. (a) Microcircuit dipole placement and orientation in the grey matter of the dlPFC in a head model, perpendicular to the cortical surface and in the middle of L2/3 (depth -725 μm). **(b)** Corresponding average potential spread of the microcircuit EEG signal to the EEG electrodes across the head. **(c)** Distribution of the difference in spectral power for depression versus healthy simulated microcircuit signals for theta-alpha band (4 – 12 Hz).

Discussion

In this study, we identified the signatures of reduced cortical inhibition in depression on EEG signals of resting-state activity using detailed models of human cortical microcircuits. Depression microcircuits with reduced SST interneuron inhibition showed an increase in absolute theta, alpha and low beta power, which involved a broadband increase together with a periodic increase in theta and low-beta activity. These EEG signatures of reduced SST interneuron inhibition were distinct from those corresponding to reducing PV interneuron inhibition. These signatures may thus be used as biomarkers to stratify depression subtypes corresponding to altered inhibition, which are particularly associated with treatment-resistant depression[50]. By simulating both spiking and EEG in detailed microcircuits, we showed that neuronal spiking had a marked preference for the phase preceding the trough of theta-alpha EEG band in both conditions. Our results provide mechanistic links between reduced SST interneuron inhibition and candidate biomarkers in EEG signals. These findings have multiple clinical applications, such as improving patient stratification and monitoring the effects of therapeutic compounds targeting SST interneuron inhibition.

Increased power of theta, alpha, and low beta bands in our simulated depression microcircuits is in agreement with several previous depression studies, and was shown to be correlated with diagnosis, severity, and treatment response[7,51–56]. Importantly, systematic reviews across psychiatric disorders showed that these band changes are most consistent in depression and thus particular to this disorder[52]. Further, increased frontal theta power is predictive of second line treatment response targeting cortical inhibition in treatment-resistant depression[55]. In addition, increased frontal theta power is seen in early depression in general and also later in treatment resistant depression, indicating a possibly consistent circuit mechanism across the lifetime of treatment-resistant depression[8,50,52–55]. Together with the several points mentioned above, our results provide support for reduced SST interneuron inhibition as a principal mechanism of treatment-resistant depression, and show that it may be detectible by a profile of increased power across the low frequency bands[52,54,57–59]. Future studies relating our simulated EEG biomarkers to experimental EEG and depression features will further establish the link to disease stage, subtype and severity. The increased aperiodic broadband power and decreased aperiodic slope in our depression microcircuits are consistent with the respective effects of increased excitation-inhibition ratio and increased baseline activity[60–62], which in our simulations resulted from reduced SST interneuron inhibition, with the opposite effect in the case of reduced PV. Increased rhythmic theta and low beta activity, but not alpha, may explain a lack of change in relative alpha power seen previously and lend more functional significance to theta and low beta frequencies[63–66]. In addition to the theta power change, we found altered theta-phase selectivity in simulated depression circuits. As previous studies have shown that theta waves modulate network excitability[67], the increased theta activity in depression microcircuits may have further functional consequences via altering cortical dynamics and processing. In summary, our results show that altered inhibition in microscale brain circuits in depression is reflected in key features of the EEG spectral density, which can be used to better stratify depression subtype and severity.

The large effect of reduced SST interneuron inhibition on low frequency resting state oscillations in our simulations is supported by the principal role of SST interneurons in modulating baseline cortical activity[8,28,33,68]. Contrarily, the lesser role of PV interneurons in governing resting activity compared to SST interneurons accounts for the less prominent effect of PV interneuron inhibition reduction on our simulated EEG spectral power[69]. We also observed a

decrease in broadband beta and gamma power (20 – 50 Hz) with decreasing PV interneuron inhibition, in agreement with hallmark optogenetic studies of PV interneuron stimulation preferentially increasing higher frequency oscillations[70]. Following spectral decomposition, we observed that reduced PV interneuron inhibition increased periodic beta activity, which was not apparent in the absolute PSD, and agrees with recent optogenetic studies[71]. Thus, by decomposing the PSD into its constituents, we further differentiated the absolute EEG signatures of reduced SST from reduced PV interneuron inhibition, highlighting this method's utility in providing EEG correlates of altered cell-type microcircuitry. Furthermore, these results provide an important validation for our model microcircuits ability to capture a wide range of modulatory effects of distinct inhibitory populations on microcircuit oscillations.

Our biophysical models of human cortical microcircuits reproduce the two most ubiquitous features of human resting state EEG: a prominent low-frequency (4 – 12 Hz) peak power and 1/f aperiodic trend [72,73]. In experimental EEG recordings, this low-frequency peak is accentuated when subjects are relaxed with their eyes closed and has the highest test-retest reliability of all spectral features[74]. While recurrent rhythmic activity generated within cortico-thalamic loops is believed to contribute strongly to scalp-measured EEG alpha, cortico-cortical interactions have also been shown to generate alpha activity in top-down processing[75]. Further, it has been shown that cortical Pyr neurons significantly contribute to and sustain theta and alpha-phasic firing due to intrinsic properties and recurrent activity[75–77]. The key features of human EEG reproduced by our microcircuit models were not explicitly constrained for, but rather emerged from the interaction of human neuronal electrical properties, synaptic connectivity, and baseline firing rates. This provides a validation of the models and indicates that they contain circuit motifs responsible for generating realistic microcircuit activity. It will be of interest in future studies to use the models for further elucidating the cellular mechanisms of oscillatory generation, especially in brain states other than rest and during cortical processing, which involve other frequency bands. As our models capture the key spectral EEG features seen *in vivo*, the simulated EEG signal magnitude can also be related to that of the recorded EEG by scaling to account for the difference between the number of neurons in our models compared to the millions of neurons that generate the recorded EEG at a given electrode[32,42].

We simulated human EEG using available detailed models of human cortical L2/3 microcircuits to serve as canonical cortical microcircuit models. These layers are closest to the

electrode and thus are important contributors to the EEG signal, especially during resting-state[78]. Previous computational studies have shown that interactions between superficial and deep layers are important contributors to electrophysiological signals in other contexts such as event-related potentials[41]. As new human cellular data becomes available, future models that also include deeper layers (4 – 6) could further refine the signatures of reduced SST interneuron inhibition in simulated resting-state EEG signals, by including the dendrites of deep pyramidal neurons and the oscillatory dynamics mediated by interactions between deep and superficial layers[40,42]. Through coupling the biophysical simulations with a forward solution using a realistic head model we showed that EEG signals would be fairly localized to the source and neighboring electrodes. This computational approach can serve to further study source localization in interpreting EEG recordings, improve inverse solutions[79], give greater physiological interpretability to statistical decomposition techniques such as independent component analysis[80] and s/eLORETA[81]. This is especially relevant in depression, where distinct brain sub-regions both serve as targets for treatment interventions, such as the lateral/medial PFC and lateral orbitofrontal cortex[82–85], and exhibit different spectral power changes in relation to diagnosing depression stage and type[54]. While we modeled and studied a single cortical region at the microcircuit scale, future studies could simulate several distinct microcircuits to examine how altered circuit mechanisms affect multi-regional interactions in depression[8].

Using detailed multi-scale models of human cortical microcircuits, we were able to characterize the EEG and spike correlates of reduced SST interneuron inhibition in depression. Previous modeling studies have shown that reduced SST interneuron inhibition in depression impairs stimulus processing due to increased baseline activity and noise[27]. Our models can serve to identify corresponding biomarkers in task EEG. The computational models we have developed also provide a powerful tool to identify the EEG biomarkers of novel therapeutic compounds and treatments for depression[17,86] via in-silico simulations to improve treatment monitoring. Finally, our models and methodology may further serve to identify EEG biomarkers of altered cellular and circuit mechanisms in other neurological diseases, such as epilepsy and schizophrenia.

Methods

Human cortical microcircuit models. We used our previous models of human cortical L2/3 microcircuits[27], consisting of 1000 neurons distributed in a 500x500x950μm^3 volume (250 to 1200μm below pia[87]). The model microcircuits included the four key neuron types in cortical L2/3: Pyramidal (Pyr), Somatostatin-expressing (SST), Parvalbumin-expressing (PV), and Vasoactive Intestinal Peptide-expressing (VIP) neurons. The proportions of the neuron types were: 80% Pyr, 5% SST, 7% PV, and 8% VIP in accordance with relative L2/3 neuron densities[88,89] and RNA-seq data[90,91]. The models were simulated using *NEURON*[92] and *LFPy*[46].

Resting-state activity simulations. We simulated eyes-closed resting-state by injecting the microcircuit models with background excitatory input representing cortical and thalamic drive, as used previously[27]. The background input was generated by random Orstein-Uhlenbeck (OU) point processes[93] placed on all neurons at the halfway point of each dendritic arbor, and 5 additional OU processes placed along the apical trunk of Pyr neurons in equal intervals, from 10% to 90% apical dendritic length. This enabled the circuit to generate recurrent activity with neuronal firing rates as measured *in vivo*[26,27,94,95]. For both healthy and depression microcircuit models (see below) we simulated 60 randomized microcircuits, for 28 seconds each.

Microcircuit models with reduced SST interneuron inhibition (depression microcircuits). We used previous models of depression microcircuits[27], with 40% reduced synaptic and tonic inhibition from SST interneurons onto all other neurons, in accordance with gene expression studies in SST interneurons in post-mortem brains from depression patients[13]. For Pyr neurons, we decreased apical tonic inhibition by 40%. For each interneuron, we decreased the relative SST contribution to tonic inhibition by 40%. To compare reduced SST from reduced PV interneuron inhibition, we then decreased synaptic and tonic inhibition from SST interneurons by 20%, 30%, 40%, 50%, 60%.

Microcircuits with reduced PV interneuron inhibition. Reduced PV interneuron inhibition was modeled by iteratively reducing synaptic and tonic inhibition from PV interneurons onto all neurons by 20%, 30%, 40%, 50% and 60%.

Simulated microcircuit EEG. We simulated layer-averaged dipole moments together with neuronal activity using *LFPy*. Corresponding EEG time series was generated using a four-sphere volume conductor model that assumes homogeneous, isotropic, and linear (frequency independent) conductivity. The radii of the four spheres representing grey matter, cerebrospinal fluid, skull, and scalp were 79 mm, 80 mm, 85 mm, and 90 mm, respectively. The conductivity for each sphere was 0.047 S/m, 1.71 S/m, 0.02 S/m, and 0.41 S/m, respectively[96]. A fixed dipole origin was placed at the midpoint of L2/3 (-725 μm), and the EEG signal was obtained via forward solution for an EEG electrode placed on the scalp surface. EEG time series were lowpass filtered at 130 Hz. EEG power spectral density (PSD) and spectrograms were calculated using Welch's method[97], with a 3s second Hanning window for PSD, and 0.5s Hanning window for spectrograms. Both analyses used 80% window overlap.

EEG periodic and aperiodic components. We decomposed EEG PSDs into periodic and aperiodic (broadband) components using tools from the FOOOF library[60]. The aperiodic component of the PSD was a 1/f function, defined by a vertical offset and exponent parameter. Periodic components representing putative oscillations were derived using up to 4 Gaussians, defined by center frequency (mean), bandwidth (variance), and power (height).

Population spiking phase preference. We calculated the instantaneous phase of EEG using tools from the *SciPy*[98] and *NumPy*[99] Python libraries. The EEG time series was bandpass filtered from 4 – 12 Hz, with 2 Hz padding on either end to avoid edge effects. A second order Butterworth filter was used to acquire filter coefficients, which were then passed to a linear digital filter applied forward and backwards to eliminate phase lag. The angle of the bandpass-filtered Hilbert transform was calculated and shifted by 180° to obtain the instantaneous phase of the signal with trough and peak corresponding to 0° and 180°, respectively. For each of the four neuron populations (Pyr, SST, PV, VIP), spike times were aggregated into a population spike vector and converted to corresponding phase of EEG. Spike phases were binned into 5° bins and the counts were summated over all circuits in each condition. To compare spike preference between conditions, bin counts were normalized by the maximal count.

Realistic head source modelling. The x-y-z components of microcircuit dipole moments generated from *LFPy* were imported into *MNE*[100] and downsampled to a 400 Hz sampling rate. The dipole was placed within L2/3 of the left dorsolateral PFC (MNI 30, -36, -42)[101], which has been implicated in depression[102]. We solved the forward solution using a three-layer boundary element model, as implemented in LFPy, corresponding to the inner skull, outer skull, and scalp with conductivities of 0.3 S/m, 0.006 S/m and 0.3 S/m, respectively. The resulting potential was calculated for a standard 60-channel simulated EEG electrode array.

Statistical tests. We used two-sample t-test to determine statistical significance where appropriate. We calculated Cohen's *d* to show effect size. We used Raileigh's test of non-uniformity to determine if populations had a non-uniform phase preference, and kurtosis to quantify variance around the preferred mean angle.

Data availability statement. All models and code will be available online upon publication.

Acknowledgements

FM, JG, and EH thank the Krembil Foundation and the Ontario Graduate Scholarship for funding support. FM and EH were also supported by a stipend award from the Department of Physiology at University of Toronto.

References

1. Chiu M, Lebenbaum M, Cheng J, de Oliveira C, Kurdyak P. The direct healthcare costs associated with psychological distress and major depression: A population-based cohort study in Ontario, Canada. PLoS ONE. 2017;12. doi:10.1371/journal.pone.0184268

2. Verduijn J, Milaneschi Y, Schoevers RA, van Hemert AM, Beekman ATF, Penninx BWJH. Pathophysiology of major depressive disorder: mechanisms involved in etiology are not associated with clinical progression. Transl Psychiatry. 2015;5: e649–e649. doi:10.1038/tp.2015.137

3. Prins J, Olivier B, Korte SM. Triple reuptake inhibitors for treating subtypes of major depressive disorder: the monoamine hypothesis revisited. Expert Opin Investig Drugs. 2011;20: 1107–1130. doi:10.1517/13543784.2011.594039

4. Al-Harbi KS. Treatment-resistant depression: therapeutic trends, challenges, and future directions. Patient Prefer Adherence. 2012;6: 369–388. doi:10.2147/PPA.S29716

5. Fitzgerald PB, Hoy KE, Anderson RJ, Daskalakis ZJ. A STUDY OF THE PATTERN OF RESPONSE TO rTMS TREATMENT IN DEPRESSION. Depress Anxiety. 2016;33: 746–753. doi:10.1002/da.22503

6. Olbrich S, Arns M. EEG biomarkers in major depressive disorder: Discriminative power and prediction of treatment response. Int Rev Psychiatry. 2013;25: 604–618. doi:10.3109/09540261.2013.816269

7. Jaworska N, Blier P, Fusee W, Knott V. Alpha power, alpha asymmetry and anterior cingulate cortex activity in depressed males and females. J Psychiatr Res. 2012;46: 1483–1491. doi:10.1016/j.jpsychires.2012.08.003

8. Northoff G, Sibille E. Why are cortical GABA neurons relevant to internal focus in depression? A cross-level model linking cellular, biochemical and neural network findings. Mol Psychiatry. 2014;19: 966–977. doi:10.1038/mp.2014.68

9. Prévot T, Sibille E. Altered GABA-mediated information processing and cognitive dysfunctions in depression and other brain disorders. Mol Psychiatry. 2021;26: 151–167. doi:10.1038/s41380-020-0727-3

10. Fuchs T, Jefferson SJ, Hooper A, Yee P-H, Maguire J, Luscher B. Disinhibition of somatostatin-positive GABAergic interneurons results in an anxiolytic and antidepressant-like brain state. Mol Psychiatry. 2017;22: 920–930. doi:10.1038/mp.2016.188

11. Lin L-C, Sibille E. Reduced brain somatostatin in mood disorders: a common pathophysiological substrate and drug target? Front Pharmacol. 2013;4: 110. doi:10.3389/fphar.2013.00110

12. Fee C, Prevot TD, Misquitta K, Knutson DE, Li G, Mondal P, et al. Behavioral deficits induced by somatostatin-positive GABA neuron silencing are rescued by alpha 5 GABA-A receptor potentiation. Int J Neuropsychopharmacol. 2021. doi:10.1093/ijnp/pyab002

13. Seney ML, Tripp A, McCune S, Lewis D, Sibille E. Laminar and Cellular Analyses of Reduced Somatostatin Gene Expression in the Subgenual Anterior Cingulate Cortex in Major Depression. Neurobiol Dis. 2015;73: 213–219. doi:10.1016/j.nbd.2014.10.005

14. Sibille E, Morris HM, Kota RS, Lewis DA. GABA-related transcripts in the dorsolateral prefrontal cortex in mood disorders. Int J Neuropsychopharmacol. 2011;14: 721–734. doi:10.1017/S1461145710001616

15. Tripp A, Kota RS, Lewis DA, Sibille E. Reduced somatostatin in subgenual anterior cingulate cortex in major depression. Neurobiol Dis. 2011;42: 116–124. doi:10.1016/j.nbd.2011.01.014

16. Guilloux J-P, Douillard-Guilloux G, Kota R, Wang X, Gardier A, Martinowich K, et al. Molecular evidence for BDNF- and GABA-related dysfunctions in the amygdala of female subjects with Major Depression. Mol Psychiatry. 2012;17: 1130–1142. doi:10.1038/mp.2011.113

17. Prevot TD, Li G, Vidojevic A, Misquitta KA, Fee C, Santrac A, et al. Novel Benzodiazepine-Like Ligands with Various Anxiolytic, Antidepressant, or Pro-Cognitive Profiles. Complex Psychiatry. 2019;5: 84–97. doi:10.1159/000496086

18. Rajkowska G, O'Dwyer G, Teleki Z, Stockmeier CA, Miguel-Hidalgo JJ. GABAergic neurons immunoreactive for calcium binding proteins are reduced in the prefrontal cortex in major depression. Neuropsychopharmacol Off Publ Am Coll Neuropsychopharmacol. 2007;32: 471–482. doi:10.1038/sj.npp.1301234

19. Solarski M, Wang H, Wille H, Schmitt-Ulms G. Somatostatin in Alzheimer's disease: A new Role for an Old Player. Prion. 2018;12: 1–8. doi:10.1080/19336896.2017.1405207

20. Mohan A, Thalamuthu A, Mather KA, Zhang Y, Catts VS, Weickert CS, et al. Differential expression of synaptic and interneuron genes in the aging human prefrontal cortex. Neurobiol Aging. 2018;70: 194–202. doi:10.1016/j.neurobiolaging.2018.06.011

21. Olejniczak P. Neurophysiologic basis of EEG. J Clin Neurophysiol Off Publ Am Electroencephalogr Soc. 2006;23: 186–189. doi:10.1097/01.wnp.0000220079.61973.6c

22. Tremblay R, Lee S, Rudy B. GABAergic interneurons in the neocortex: From cellular properties to circuits. Neuron. 2016;91: 260–292. doi:10.1016/j.neuron.2016.06.033

23. Ali AB, Thomson AM. Synaptic alpha 5 subunit-containing GABAA receptors mediate IPSPs elicited by dendrite-preferring cells in rat neocortex. Cereb Cortex N Y N 1991. 2008;18: 1260–1271. doi:10.1093/cercor/bhm160

24. Silberberg G, Markram H. Disynaptic Inhibition between Neocortical Pyramidal Cells Mediated by Martinotti Cells. Neuron. 2007;53: 735–746. doi:10.1016/j.neuron.2007.02.012

25. Obermayer J, Heistek TS, Kerkhofs A, Goriounova NA, Kroon T, Baayen JC, et al. Lateral inhibition by Martinotti interneurons is facilitated by cholinergic inputs in human and mouse neocortex. Nat Commun. 2018;9: 4101. doi:10.1038/s41467-018-06628-w

26. Gentet LJ, Kremer Y, Taniguchi H, Huang ZJ, Staiger JF, Petersen CCH. Unique functional properties of somatostatin-expressing GABAergic neurons in mouse barrel cortex. Nat Neurosci. 2012;15: 607–612. doi:10.1038/nn.3051

27. Yao HK, Guet-McCreight A, Mazza F, Chameh HM, Prevot TD, Griffiths J, et al. Reduced inhibition in depression impairs stimulus processing in human cortical microcircuits. bioRxiv. 2021; 2021.02.17.431698. doi:10.1101/2021.02.17.431698

28. Chen G, Zhang Y, Li X, Zhao X, Ye Q, Lin Y, et al. Distinct Inhibitory Circuits Orchestrate Cortical beta and gamma Band Oscillations. Neuron. 2017;96: 1403-1418.e6. doi:10.1016/j.neuron.2017.11.033

29. Huang P, Xiang X, Chen X, Li H. Somatostatin Neurons Govern Theta Oscillations Induced by Salient Visual Signals. Cell Rep. 2020;33: 108415. doi:10.1016/j.celrep.2020.108415

30. Funk CM, Peelman K, Bellesi M, Marshall W, Cirelli C, Tononi G. Role of Somatostatin-Positive Cortical Interneurons in the Generation of Sleep Slow Waves. J Neurosci. 2017;37: 9132–9148. doi:10.1523/JNEUROSCI.1303-17.2017

31. Jiang H, Popov T, Jylänki P, Bi K, Yao Z, Lu Q, et al. Predictability of depression severity based on posterior alpha oscillations. Clin Neurophysiol Off J Int Fed Clin Neurophysiol. 2016;127: 2108–2114. doi:10.1016/j.clinph.2015.12.018

32. Murakami S, Okada Y. Contributions of principal neocortical neurons to magnetoencephalography and electroencephalography signals. J Physiol. 2006;575: 925–936. doi:10.1113/jphysiol.2006.105379

33. Womelsdorf T, Valiante TA, Sahin NT, Miller KJ, Tiesinga P. Dynamic circuit motifs underlying rhythmic gain control, gating and integration. Nat Neurosci. 2014;17: 1031–1039. doi:10.1038/nn.3764

34. Dehghani N, Peyrache A, Telenczuk B, Le Van Quyen M, Halgren E, Cash SS, et al. Dynamic Balance of Excitation and Inhibition in Human and Monkey Neocortex. Sci Rep. 2016;6: 23176. doi:10.1038/srep23176

35. Quyen MLV, Muller LE, Telenczuk B, Halgren E, Cash S, Hatsopoulos NG, et al. High-frequency oscillations in human and monkey neocortex during the wake–sleep cycle. Proc Natl Acad Sci. 2016;113: 9363–9368. doi:10.1073/pnas.1523583113

36. Gardner RJ, Hughes SW, Jones MW. Differential Spike Timing and Phase Dynamics of Reticular Thalamic and Prefrontal Cortical Neuronal Populations during Sleep Spindles. J Neurosci. 2013;33: 18469–18480. doi:10.1523/JNEUROSCI.2197-13.2013

37. Averkin RG, Szemenyei V, Bordé S, Tamás G. Identified Cellular Correlates of Neocortical Ripple and High-Gamma Oscillations during Spindles of Natural Sleep. Neuron. 2016;92: 916–928. doi:10.1016/j.neuron.2016.09.032

38. McGinn RJ, Valiante TA. Phase–Amplitude Coupling and Interlaminar Synchrony Are Correlated in Human Neocortex. J Neurosci. 2014;34: 15923–15930. doi:10.1523/JNEUROSCI.2771-14.2014

39. Fedele T, Boran E, Chirkov V, Hilfiker P, Grunwald T, Stieglitz L, et al. Dataset of spiking and LFP activity invasively recorded in the human amygdala during aversive dynamic stimuli. Sci Data. 2021;8: 9. doi:10.1038/s41597-020-00790-x

40. Florez CM, McGinn RJ, Lukankin V, Marwa I, Sugumar S, Dian J, et al. In vitro recordings of human neocortical oscillations. Cereb Cortex N Y N 1991. 2015;25: 578–597. doi:10.1093/cercor/bht235

41. Kohl C, Parviainen T, Jones SR. Neural Mechanisms Underlying Human Auditory Evoked Responses Revealed By Human Neocortical Neurosolver. Brain Topogr. 2021 [cited 30 Nov 2021]. doi:10.1007/s10548-021-00838-0

42. Jones SR, Pritchett DL, Sikora MA, Stufflebeam SM, Hämäläinen M, Moore CI. Quantitative analysis and biophysically realistic neural modeling of the MEG mu rhythm: rhythmogenesis and modulation of sensory-evoked responses. J Neurophysiol. 2009;102: 3554–3572. doi:10.1152/jn.00535.2009

43. Mohan H, Verhoog MB, Doreswamy KK, Eyal G, Aardse R, Lodder BN, et al. Dendritic and Axonal Architecture of Individual Pyramidal Neurons across Layers of Adult Human Neocortex. Cereb Cortex N Y N 1991. 2015;25: 4839–4853. doi:10.1093/cercor/bhv188

44. Seeman SC, Campagnola L, Davoudian PA, Hoggarth A, Hage TA, Bosma-Moody A, et al. Sparse recurrent excitatory connectivity in the microcircuit of the adult mouse and human cortex. Slutsky I, Marder E, Sjöström PJ, editors. eLife. 2018;7: e37349. doi:10.7554/eLife.37349

45. Chameh HM, Rich S, Wang L, Chen F-D, Zhang L, Carlen PL, et al. Sag currents are a major contributor to human pyramidal cell intrinsic differences across cortical layers. bioRxiv. 2020; 748988. doi:10.1101/748988

46. Hagen E, Næss S, Ness TV, Einevoll GT. Multimodal modeling of neural network activity: computing LFP, ECoG, EEG and MEG signals with LFPy2.0. bioRxiv. 2018; 281717. doi:10.1101/281717

47. Mäki-Marttunen T, Krull F, Bettella F, Hagen E, Næss S, Ness TV, et al. Alterations in Schizophrenia-Associated Genes Can Lead to Increased Power in Delta Oscillations. Cereb Cortex. 2019;29: 875–891. doi:10.1093/cercor/bhy291

48. Groppe DM, Bickel S, Keller CJ, Jain SK, Hwang ST, Harden C, et al. Dominant frequencies of resting human brain activity as measured by the electrocorticogram. NeuroImage. 2013;79: 223–233. doi:10.1016/j.neuroimage.2013.04.044

49. He BJ. Scale-free brain activity: past, present, and future. Trends Cogn Sci. 2014;18: 480–487. doi:10.1016/j.tics.2014.04.003

50. Fee C, Banasr M, Sibille E. Somatostatin-Positive Gamma-Aminobutyric Acid Interneuron Deficits in Depression: Cortical Microcircuit and Therapeutic Perspectives. Biol Psychiatry. 2017;82: 549–559. doi:10.1016/j.biopsych.2017.05.024

51. Fernández-Palleiro P, Rivera-Baltanás T, Rodrigues-Amorim D, Fernández-Gil S, del Carmen Vallejo-Curto M, Álvarez-Ariza M, et al. Brainwaves Oscillations as a Potential Biomarker for Major Depression Disorder Risk. Clin EEG Neurosci. 2020;51: 3–9. doi:10.1177/1550059419876807

52. Newson JJ, Thiagarajan TC. EEG Frequency Bands in Psychiatric Disorders: A Review of Resting State Studies. Front Hum Neurosci. 2018;12: 521. doi:10.3389/fnhum.2018.00521

53. Arns M, Etkin A, Hegerl U, Williams LM, DeBattista C, Palmer DM, et al. Frontal and rostral anterior cingulate (rACC) theta EEG in depression: implications for treatment outcome? Eur Neuropsychopharmacol J Eur Coll Neuropsychopharmacol. 2015;25: 1190–1200. doi:10.1016/j.euroneuro.2015.03.007

54. Grin-Yatsenko VA, Baas I, Ponomarev VA, Kropotov JD. Independent component approach to the analysis of EEG recordings at early stages of depressive disorders. Clin Neurophysiol. 2010;121: 281–289. doi:10.1016/j.clinph.2009.11.015

55. Bailey NW, Hoy KE, Rogasch NC, Thomson RH, McQueen S, Elliot D, et al. Responders to rTMS for depression show increased fronto-midline theta and theta connectivity compared to non-responders. Brain Stimulat. 2018;11: 190–203. doi:10.1016/j.brs.2017.10.015

56. Bruder GE, Sedoruk JP, Stewart JW, McGrath PJ, Quitkin FM, Tenke CE. Electroencephalographic Alpha Measures Predict Therapeutic Response to a Selective Serotonin Reuptake Inhibitor Antidepressant: Pre- and Post-Treatment Findings. Biol Psychiatry. 2008;63: 1171–1177. doi:10.1016/j.biopsych.2007.10.009

57. de Aguiar Neto FS, Rosa JLG. Depression biomarkers using non-invasive EEG: A review. Neurosci Biobehav Rev. 2019;105: 83–93. doi:10.1016/j.neubiorev.2019.07.021

58. Olbrich S, Arns M. EEG biomarkers in major depressive disorder: discriminative power and prediction of treatment response. Int Rev Psychiatry Abingdon Engl. 2013;25: 604–618. doi:10.3109/09540261.2013.816269

59. Smith DF. Quest for Biomarkers of Treatment-Resistant Depression: Shifting the Paradigm Toward Risk. Front Psychiatry. 2013;4. doi:10.3389/fpsyt.2013.00057

60. Donoghue T, Haller M, Peterson EJ, Varma P, Sebastian P, Gao R, et al. Parameterizing neural power spectra into periodic and aperiodic components. Nat Neurosci. 2020;23: 1655–1665. doi:10.1038/s41593-020-00744-x

61. Gao R, Peterson EJ, Voytek B. Inferring synaptic excitation/inhibition balance from field potentials. NeuroImage. 2017;158: 70–78. doi:10.1016/j.neuroimage.2017.06.078

62. Podvalny E, Noy N, Harel M, Bickel S, Chechik G, Schroeder CE, et al. A unifying principle underlying the extracellular field potential spectral responses in the human cortex. J Neurophysiol. 2015;114: 505–519. doi:10.1152/jn.00943.2014

63. Knott V, Mahoney C, Kennedy S, Evans K. EEG power, frequency, asymmetry and coherence in male depression. Psychiatry Res Neuroimaging. 2001;106: 123–140. doi:10.1016/S0925-4927(00)00080-9

64. Morgan ML, Witte EA, Cook IA, Leuchter AF, Abrams M, Siegman B. Influence of age, gender, health status, and depression on quantitative EEG. Neuropsychobiology. 2005;52: 71–76. doi:10.1159/000086608

65. Korb AS, Cook IA, Hunter AM, Leuchter AF. Brain electrical source differences between depressed subjects and healthy controls. Brain Topogr. 2008;21: 138–146. doi:10.1007/s10548-008-0070-5

66. Cook IA, Hunter AM, Korb AS, Leuchter AF. Do prefrontal midline electrodes provide unique neurophysiologic information in Major Depressive Disorder? J Psychiatr Res. 2014;53: 69–75. doi:10.1016/j.jpsychires.2014.01.018

67. Buzsáki G. Theta oscillations in the hippocampus. Neuron. 2002;33: 325–340. doi:10.1016/s0896-6273(02)00586-x

68. Gentet LJ, Kremer Y, Taniguchi H, Huang ZJ, Staiger JF, Petersen CCH. Unique functional properties of somatostatin-expressing GABAergic neurons in mouse barrel cortex. Nat Neurosci. 2012;15: 607–612. doi:10.1038/nn.3051

69. Sohal VS, Zhang F, Yizhar O, Deisseroth K. Parvalbumin neurons and gamma rhythms enhance cortical circuit performance. Nature. 2009;459: 698–702. doi:10.1038/nature07991

70. Cardin JA, Carlén M, Meletis K, Knoblich U, Zhang F, Deisseroth K, et al. Driving fast-spiking cells induces gamma rhythm and controls sensory responses. Nature. 2009;459: 663–667. doi:10.1038/nature08002

71. Chen G, Zhang Y, Li X, Zhao X, Ye Q, Lin Y, et al. Distinct Inhibitory Circuits Orchestrate Cortical beta and gamma Band Oscillations. Neuron. 2017;96: 1403-1418.e6. doi:10.1016/j.neuron.2017.11.033

72. Nunez PL, Srinivasan R. Electric fields of the brain: the neurophysics of EEG. 2nd ed. Oxford ; New York: Oxford University Press; 2006.

73. Ouyang G, Hildebrandt A, Schmitz F, Herrmann CS. Decomposing alpha and 1/f brain activities reveals their differential associations with cognitive processing speed. Neuroimage. 2020;205. doi:10.1016/j.neuroimage.2019.116304

74. Gasser T, Bächer P, Steinberg H. Test-retest reliability of spectral parameters of the EEG. Electroencephalogr Clin Neurophysiol. 1985;60: 312–319. doi:10.1016/0013-4694(85)90005-7

75. Halgren M, Ulbert I, Bastuji H, Fabó D, Erőss L, Rey M, et al. The generation and propagation of the human alpha rhythm. Proc Natl Acad Sci. 2019;116: 23772–23782. doi:10.1073/pnas.1913092116

76. Silva LR, Amitai Y, Connors BW. Intrinsic oscillations of neocortex generated by layer 5 pyramidal neurons. Science. 1991;251: 432–435. doi:10.1126/science.1824881

77. Connors BW, Gutnick MJ. Intrinsic firing patterns of diverse neocortical neurons. Trends Neurosci. 1990;13: 99–104. doi:10.1016/0166-2236(90)90185-D

78. Buzsáki G, Anastassiou CA, Koch C. The origin of extracellular fields and currents--EEG, ECoG, LFP and spikes. Nat Rev Neurosci. 2012;13: 407–420. doi:10.1038/nrn3241

79. Grech R, Cassar T, Muscat J, Camilleri KP, Fabri SG, Zervakis M, et al. Review on solving the inverse problem in EEG source analysis. J NeuroEngineering Rehabil. 2008;5: 25. doi:10.1186/1743-0003-5-25

80. Makeig S, Bell AJ, Jung T-P, Sejnowski TJ. Independent Component Analysis of Electroencephalographic Data. : 7.

81. Pascual-Marqui RD, Lehmann D, Koukkou M, Kochi K, Anderer P, Saletu B, et al. Assessing interactions in the brain with exact low-resolution electromagnetic tomography. Philos Trans R Soc Math Phys Eng Sci. 2011;369: 3768–3784. doi:10.1098/rsta.2011.0081

82. Feffer K, Fettes P, Giacobbe P, Daskalakis ZJ, Blumberger DM, Downar J. 1Hz rTMS of the right orbitofrontal cortex for major depression: Safety, tolerability and clinical outcomes. Eur Neuropsychopharmacol J Eur Coll Neuropsychopharmacol. 2018;28: 109–117. doi:10.1016/j.euroneuro.2017.11.011

83. Li Y, Wang L, Jia M, Guo J, Wang H, Wang M. The effects of high-frequency rTMS over the left DLPFC on cognitive control in young healthy participants. PLoS ONE. 2017;12. doi:10.1371/journal.pone.0179430

84. Bakker N, Shahab S, Giacobbe P, Blumberger DM, Daskalakis ZJ, Kennedy SH, et al. rTMS of the Dorsomedial Prefrontal Cortex for Major Depression: Safety, Tolerability, Effectiveness, and Outcome Predictors for 10 Hz Versus Intermittent Theta-burst Stimulation. Brain Stimulat. 2015;8: 208–215. doi:10.1016/j.brs.2014.11.002

85. Fettes P, Schulze L, Downar J. Cortico-Striatal-Thalamic Loop Circuits of the Orbitofrontal Cortex: Promising Therapeutic Targets in Psychiatric Illness. Front Syst Neurosci. 2017;11. doi:10.3389/fnsys.2017.00025

86. Krystal JH, Abdallah CG, Sanacora G, Charney DS, Duman RS. Ketamine: A Paradigm Shift for Depression Research and Treatment. Neuron. 2019;101: 774–778. doi:10.1016/j.neuron.2019.02.005

87. Mohan H, Verhoog MB, Doreswamy KK, Eyal G, Aardse R, Lodder BN, et al. Dendritic and Axonal Architecture of Individual Pyramidal Neurons across Layers of Adult Human Neocortex. Cereb Cortex. 2015;25: 4839–4853. doi:10.1093/cercor/bhv188

88. Hashemi E, Ariza J, Rogers H, Noctor SC, Martínez-Cerdeño V. The Number of Parvalbumin-Expressing Interneurons Is Decreased in the Prefrontal Cortex in Autism. Cereb Cortex N Y N 1991. 2017;27: 1931–1943. doi:10.1093/cercor/bhw021

89. Krienen FM, Goldman M, Zhang Q, C. H. del Rosario R, Florio M, Machold R, et al. Innovations present in the primate interneuron repertoire. Nature. 2020;586: 262–269. doi:10.1038/s41586-020-2781-z

90. 2010 Allen Institute for Brain Science. Allen Human Brain Atlas. Available from: human.brain-map.org. [cited 19 Apr 2021]. Available: https://www.google.com/search?q=2010+Allen+Institute+for+Brain+Science.+Allen+Human+Brain+Atlas.+Available+from%3A+human.brain-map.org.&oq=2010+Allen+Institute+for+Brain+Science.+Allen+Human+Brain+Atlas.+Available+from%3A+human.brain-map.org.&aqs=chrome..69i57.422j0j4&sourceid=chrome&ie=UTF-8

91. Hodge RD, Bakken TE, Miller JA, Smith KA, Barkan ER, Graybuck LT, et al. Conserved cell types with divergent features in human versus mouse cortex. Nature. 2019;573: 61–68. doi:10.1038/s41586-019-1506-7

92. Carnevale T, Hines M, Hines M, Hines M. The NEURON Book. Cambridge University Press; 2006.

93. Destexhe A, Rudolph M, Fellous JM, Sejnowski TJ. Fluctuating synaptic conductances recreate in vivo-like activity in neocortical neurons. Neuroscience. 2001;107: 13–24. doi:10.1016/s0306-4522(01)00344-x

94. Teleńczuk B, Dehghani N, Le Van Quyen M, Cash SS, Halgren E, Hatsopoulos NG, et al. Local field potentials primarily reflect inhibitory neuron activity in human and monkey cortex. Sci Rep. 2017;7: 40211. doi:10.1038/srep40211

95. Yu J, Hu H, Agmon A, Svoboda K. Recruitment of GABAergic Interneurons in the Barrel Cortex during Active Tactile Behavior. Neuron. 2019;104: 412-427.e4. doi:10.1016/j.neuron.2019.07.027

96. McCann H, Pisano G, Beltrachini L. Variation in Reported Human Head Tissue Electrical Conductivity Values. Brain Topogr. 2019;32: 825–858. doi:10.1007/s10548-019-00710-2

97. Welch P. The use of fast Fourier transform for the estimation of power spectra: A method based on time averaging over short, modified periodograms. IEEE Trans Audio Electroacoustics. 1967;15: 70–73. doi:10.1109/TAU.1967.1161901

98. Virtanen P, Gommers R, Oliphant TE, Haberland M, Reddy T, Cournapeau D, et al. SciPy 1.0: fundamental algorithms for scientific computing in Python. Nat Methods. 2020;17: 261–272. doi:10.1038/s41592-019-0686-2

99. Harris CR, Millman KJ, van der Walt SJ, Gommers R, Virtanen P, Cournapeau D, et al. Array programming with NumPy. Nature. 2020;585: 357–362. doi:10.1038/s41586-020-2649-2

100. Gramfort A, Luessi M, Larson E, Engemann DA, Strohmeier D, Brodbeck C, et al. MEG and EEG data analysis with MNE-Python. Front Neurosci. 2013;7. doi:10.3389/fnins.2013.00267

101. McBride D, Barrett SP, Kelly JT, Aw A, Dagher A. Effects of expectancy and abstinence on the neural response to smoking cues in cigarette smokers: an fMRI study. Neuropsychopharmacol Off Publ Am Coll Neuropsychopharmacol. 2006;31: 2728–2738. doi:10.1038/sj.npp.1301075

102. Koenigs M, Grafman J. The functional neuroanatomy of depression: Distinct roles for ventromedial and dorsolateral prefrontal cortex. Behav Brain Res. 2009;201: 239–243. doi:10.1016/j.bbr.2009.03.004